Biochemical and Biophysical Research Communications 449 (2014) 241–247

Contents lists available at ScienceDirect

Biochemical and Biophysical Research Communications

journal homepage: www.elsevier.com/locate/ybbrc

Alpha-smooth muscle actin expression identifies subpopulations of mouse lymph node non-hematopoietic cells

Khongorzul Togoo, Yousuke Takahama *, Kensuke Takada *

Division of Experimental Immunology, Institute for Genome Research, University of Tokushima, Tokushima 770-8503, Japan

ARTICLE INFO

Article history:
Received 4 May 2014
Available online 17 May 2014

Keywords:
Lymph node
Stromal cell
Alpha-smooth muscle actin
Perivascular cell

ABSTRACT

Significant attention has been given to the role played by non-hematopoietic cells in the immune organs, including the lymph nodes, in hopes of understanding the development, maintenance, and regulation of the immune system. However, the molecular and cellular characterization of non-hematopoietic cells is still in its infancy. Here we show that non-hematopoietic cells in mouse lymph nodes can be fractionated into previously unidentified subpopulations according to the transgenic reporter expression of alpha-smooth muscle actin (αSMA). αSMA$^+$ non-hematopoietic cells were predominantly detected in gp38$^+$CD31$^-$ and gp38$^-$CD31$^-$ cells. Molecular expression profiles suggest similarities between αSMA$^+$gp38$^+$CD31$^-$ and αSMA$^-$gp38$^+$CD31$^-$ subpopulations and dissimilarities between αSMA$^+$gp38$^-$CD31$^-$ and αSMA$^-$gp38$^-$CD31$^-$ subpopulations. The results indicate that αSMA is a useful marker for further understanding the molecular and cellular characteristics of non-hematopoietic cells in the lymph nodes.

1. Introduction

The lymph nodes play an essential role in the orchestration of immune responses in mammalian species, including human. Various non-hematopoietic cells structurally organize the lymph nodes and functionally provide the stromal microenvironments for coordinating the immune responses by hematopoietic cells. It has been shown that the lymph node non-hematopoietic cells can be subdivided into four distinct populations according to the expression of the podocyte marker gp38 (podoplanin) and the endothelial cell marker CD31 (PECAM1). The gp38$^+$CD31$^-$ cells include fibroblastic reticular cells (FRCs), which form a three-dimensional network in the T cell zones and regulate the homeostasis and trafficking of T cells [1]. The gp38$^+$CD31$^+$ and gp38$^-$CD31$^+$ cells contain lymphatic endothelial cells (LECs) and blood ECs (BECs), respectively, which critically regulate the egress and entry of lymphocytes [2]. However, the molecular and cellular characterization of non-hematopoietic cells in the lymph nodes is still in its infancy.

Alpha-smooth muscle actin (αSMA) is expressed in cells of smooth muscle lineage in various organs. The αSMA expression is often associated with perivascular cells (PVCs), including pericytes surrounding microvessels and vascular smooth muscle cells surrounding large vessels [3,4]. Although αSMA-expressing cells have been detected also in the lymph nodes [5], the molecular and cellular characteristics of αSMA$^+$ cells in the lymph nodes are unclear, especially in the context of well-studied non-hematopoietic populations that are subdivided according to the expression of gp38 and CD31.

In the present study, we examined αSMA expression in lymph nodes using αSMA-GFP-transgenic mice. Green fluorescent protein (GFP) expression in those mice faithfully reflects the specific expression of αSMA and can identify nonvascular and vascular smooth muscle cells, including renal glomerular mesangial cells, and a small population of bone marrow stromal cells [6]. Our results show that GFP$^+$ cells in the lymph nodes of αSMA-GFP-transgenic mice mostly comprise non-hematopoietic cells and at the same time contain a small population of hematopoietic cells, which represent macrophages that have likely acquired GFP proteins from the non-hematopoietic αSMA$^+$ cells. Interestingly, αSMA-GFP expression in the lymph nodes made possible the identification of subpopulations of gp38$^+$CD31$^-$ and gp38$^-$CD31$^-$ non-hematopoietic cells. The results have enabled the identification of hitherto unknown subpopulations of non-hematopoietic cells in the lymph nodes.

Abbreviations: FRC, fibroblastic reticular cell; LEC, lymphatic endothelial cell; BEC, blood endothelial cell; αSMA, alpha-smooth muscle actin; PVC, perivascular cell; HEV, high endothelial venule.

* Corresponding authors. Fax: +81 88 633 9453.
E-mail addresses: takahama@genome.tokushima-u.ac.jp (Y. Takahama), takada@genome.tokushima-u.ac.jp (K. Takada).

http://dx.doi.org/10.1016/j.bbrc.2014.05.023
0006-291X/

2. Materials and methods

2.1. Mice

αSMA-GFP-transgenic mice in C57BL/6 (B6) background, which express GFP under the control of smooth muscle type alpha-actin (αSMA) promoter, were originally from the National Eye Institute, National Institutes of Health, USA [6]. B6 mice were obtained from SLC (Shizuoka, Japan), whereas B6-Ly5.1 mice were maintained in our laboratory. The mice were maintained under specific pathogen-free conditions in our animal facility. The experiments were conducted under the approval of the Institutional Animal Care and Use Committee of University of Tokushima.

2.2. Bone marrow chimeras

Bone marrow cells were depleted of T cells by using anti-Thy1.2 magnetic beads (Miltenyi Biotec). Recipient mice were lethally irradiated (10 Gy) and injected intravenously with $1–2 \times 10^7$ T-cell-depleted bone marrow cells. The lymph nodes were analyzed 8–11 weeks after the reconstitution.

2.3. Enzymatic digestion of lymph nodes

Cervical, axillary, brachial, inguinal, and mesenteric lymph nodes were dissected into small pieces and incubated in RPMI-1640 medium containing 0.2 mg/ml collagenase P, 0.8 mg/ml dispase (Roche), and 0.1 mg/ml DNase I (Roche) at 37 °C [7]. To enrich non-hematopoietic cells, leukocytes and erythroid cells were depleted by incubating the cell suspension with anti-CD45 and anti-TER119 microbeads and passing over a MACS column (Miltenyi Biotec).

2.4. Flow cytometric analysis and cell sorting

Anti-FcγR monoclonal antibody (clone 2.4G2) was added before antibody staining to block FcγR-mediated binding of staining antibodies to the cells. Collagenase-digested lymph node cells were incubated for 20 min on ice with fluorochrome-conjugated antibodies (eBioscience). We used antibodies specific for CD11b, CD11c, CD29, CD31, CD44, CD45, CD45.1, CD45.2, CD54, CD90 (Thy-1), CD105, CD106 (VCAM-1), CD326 (EpCAM), gp38, I-A^b, LTβR, PDGFRα, PDGFRβ, and the TER119 determinant. Cells were resuspended in phosphate-buffered saline (PBS) containing 5 μM propidium iodide (PI) to exclude dead cells. Multicolor flow cytometric analysis and cell sorting were performed using FACSAria II (BD Biosciences). Data were analyzed by using FlowJo software (Tree Star).

2.5. Quantitative RT-PCR analysis

Total RNA prepared with an RNeasy Plus Micro Kit (Qiagen) was reverse-transcribed with oligo-dT primer and SuperScript III reverse transcriptase (Invitrogen). Quantitative real-time PCR was performed using SYBR Premix Ex Taq (TaKaRa) on a 7900HT Fast Real-Time PCR System (Applied Biosystems). The amplified products were confirmed to be single bands by gel electrophoresis and normalized to the amount of glyceraldehyde-3-phosphate dehydrogenase (GAPDH) amplification products. Primer sequences are listed in Supplementary Table S1.

2.6. Immunofluorescence analysis

Tissues were fixed in 4% paraformaldehyde, incubated in 10–30% sucrose in PBS, embedded in OCT compound (Sakura Tissue-Tek), and frozen. Cryostat sections (5-μm-thick) were incubated with biotinylated antibodies specific for CD3, B220, CD11b, PNAd, and gp38, and then with AlexaFluor 633-conjugated streptavidin (Invitrogen). Sections were also stained with ER-TR7 followed by AlexaFluor 546-conjugated anti-rat IgG antibody (Invitrogen). Images were analyzed with a TSC SP8 confocal laser-scanning microscope and Leica Confocal software (LAS AF Version 3.2.1, Leica).

2.7. Statistical analysis

For comparison of two groups, *p*-values were obtained using the Student's *t*-test (unpaired, two-tailed, 95% confidence interval) and statistical significance was denoted by $p < 0.05$, $p < 0.01$, and $p < 0.001$, which were shown as *, **, and ***, respectively. Statistical analysis was performed with Prism 4.0 (GraphPad Software).

3. Results

3.1. αSMA-GFP expression in lymph nodes

It was reported that GFP expression in αSMA-GFP-transgenic mice faithfully reflects the specific expression of αSMA and can identify vascular and nonvascular smooth muscle cells as well as a small population of bone marrow stromal cells [6]. In order to characterize αSMA-expressing cells in the lymph nodes, we first examined GFP expression in paraformaldehyde-fixed sections of inguinal lymph nodes from αSMA-GFP-transgenic mice. GFP signals, which were detectable in various areas of the lymph nodes (Fig. 1A), were distributed in the T cell area, where $CD3^+$ T cells were accumulated, and the non-T non-B area, where neither $CD3^+$ T cells nor $B220^+$ B cells were enriched (Fig. 1B–D). GFP signals were less pronounced in B cell follicles where $B220^+$ B cells were accumulated (Fig. 1A and C). Some GFP signals in the non-T non-B area closely surrounded PNAd-expressing high endothelial venules (HEVs), in the same manner as that observed in PVCs (Fig. 1E). Other GFP signals in the non-T non-B area were heterogeneous with regard to the co-expression with gp38; some GFP signals merged with gp38 signals (Fig. 1F, arrowheads) whereas others did not (Fig. 1F, arrows), and many $gp38^+$ cells were negative for GFP expression (Fig. 1F, asterisks). These results agreed with a previous report showing that αSMA-expressing cells were detectable in the lymph nodes [5], and indicated that αSMA-GFP-expressing cells in the lymph nodes were heterogeneous with regard to the localization and the co-expression with gp38.

3.2. Flow cytometric analysis of αSMA-GFP-expressing cells in lymph nodes

We next characterized αSMA-GFP-expressing cells in the lymph nodes using flow cytometry. A mixture of cervical, axillary, brachial, inguinal, and mesenteric lymph nodes were digested with collagenase P, dispase, and DNase I. Cells were multi-color-stained for gp38 and CD31 as well as for the leukocyte marker CD45 and the erythrocyte marker TER119. GFP^+ cells were detectable in approximately 0.05–0.1% of viable $TER119^-$ non-erythroid cells (Fig. 2 top panels, Table 1). Interestingly, the GFP^+ cells were clearly heterogeneous with regard to the expression intensity of GFP, and thus could be subdivided into GFPhigh (GFP(hi)) and GFPlow (GFP(lo)) cells (Fig. 2 top and middle panels). The majority of the GFPhigh lymph node cells were $TER119^-CD45^-$ non-hematopoietic cells, whereas the GFPlow cells contained both $TER119^-CD45^-$ non-hematopoietic cells and $TER119^-CD45^+$ leukocytes (Fig. 2 middle panels). Both GFP^{high} and GFP^{low} non-hematopoietic cells were predominantly

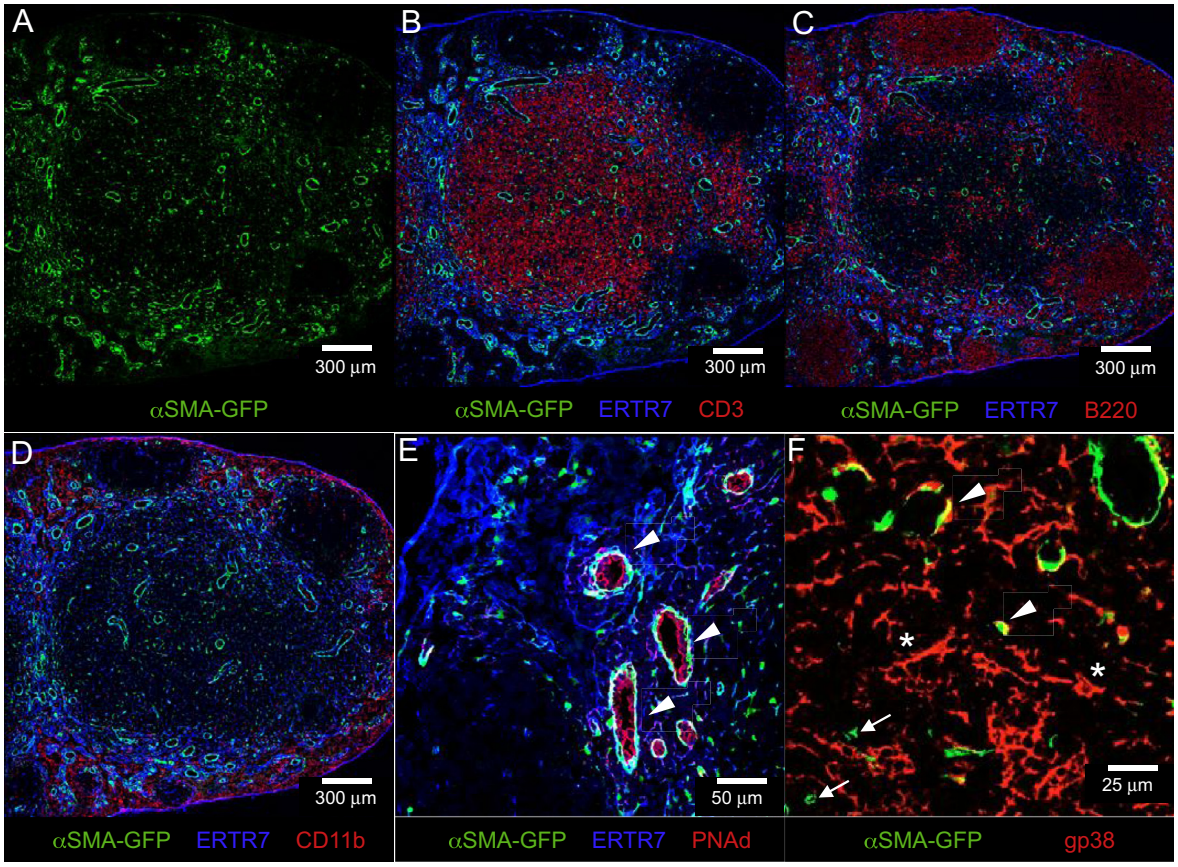

Fig. 1. Immunofluorescence analysis of GFP-expressing cells in the lymph nodes of αSMA-GFP-transgenic mice. Inguinal lymph nodes from 8-week-old mice were multi-color analyzed for GFP and indicated molecules. Representative images from two independent analyses are shown. Arrowheads indicate PNAd$^+$ HEVs surrounded by αSMA-GFP$^+$ cells (E). GFP$^+$gp38$^+$ (arrowheads), GFP$^+$gp38$^-$ (arrows), and GFP$^-$gp38$^-$ (asterisks) signals are shown (F).

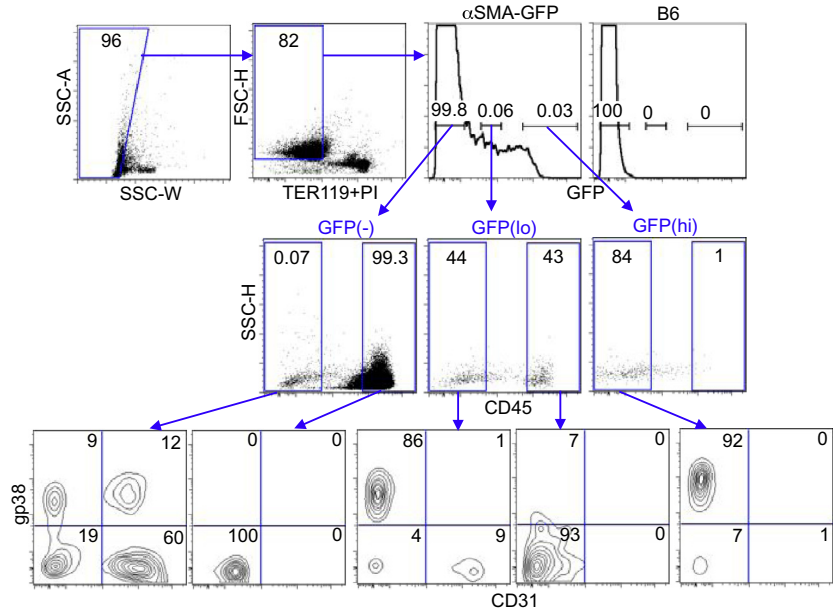

Fig. 2. Flow cytometric analysis of GFP-expressing cells in the lymph nodes of αSMA-GFP-transgenic mice. Collagenase-digested lymph node cells were obtained from 9- to 10-week-old αSMA-GFP and B6 mice. The SSC-W versus SSC-A plot was analyzed to exclude cellular aggregates, whereas the TER119 + PI versus FSC-H plot was analyzed to exclude erythroid cells, dead cells, and non-cellular debris. Numbers indicate frequency of cells within indicated areas. Shown are representative results from four independent experiments.

gp38$^+$CD31$^-$, whereas GFP$^-$ non-hematopoietic cells contained four subpopulations that could be distinguished according to the expression of gp38 and CD31 (Fig. 2 bottom panels, Table 1). GFPhigh non-hematopoietic cells contained a small fraction of gp38$^-$CD31$^-$ cells, whereas GFPlow non-hematopoietic cells contained small fractions of gp38$^-$CD31$^-$ cells and gp38$^-$CD31$^+$

Table 1
Composition of lymph node cells from αSMA-GFP-transgenic mice.

PI-TER119-cells			Frequency (%)	Cell number ($\times 10^3$/mouse)
			100	63,550 ± 6794
GFP(−)			99.8 ± 0.02	63,467 ± 6776
	$CD45^+$		99.5 ± 0.08	63,165 ± 6695
	$CD45^-$		0.06 ± 0.003	40 ± 5
		$gp38^+CD31^-$	9 ± 0.7	4 ± 0.6
		$gp38^-CD31^-$	20 ± 1	8 ± 1
		$gp38^-CD31^+$	60 ± 2	24 ± 3
		$gp38^+CD31^+$	10 ± 1	4 ± 1
GFP(lo)			0.04 ± 0.007	26 ± 7
	$CD45^+$		56 ± 6	13 ± 2
	$CD45^-$		34 ± 5	9 ± 3
		$gp38^+CD31^-$	76 ± 5	7 ± 3
		$gp38^-CD31^-$	8 ± 2	0.5 ± 0.1
		$gp38^-CD31^+$	15 ± 3	1 ± 0.3
GFP(hi)			0.02 ± 0.005	12 ± 4
	$CD45^+$		1.8 ± 0.6	0.2 ± 0.09
	$CD45^-$		83 ± 2	10 ± 3
		$gp38^+CD31^-$	91 ± 1	9 ± 3
		$gp38^-CD31^-$	7 ± 0.6	0.6 ± 0.2

Lymph node cells were obtained from cervical, axillary, brachial, inguinal, and mesenteric lymph nodes.
Means and SEMs ($n = 4$) of absolute cell numbers are shown.

cells (Fig. 2 bottom panels, Table 1). These results indicated that GFP^+ lymph node cells contained GFP^{high} and GFP^{low} cells and that the GFP^{high} lymph node cells were mostly non-hematopoietic cells whereas the GFP^{low} cells contained both non-hematopoietic and hematopoietic cells. The GFP^{high} and GFP^{low} non-hematopoietic cells were enriched with $gp38^+CD31^-$ cells.

3.3. αSMA-GFP^{low} hematopoietic cells are macrophages

Analysis of the isolated $GFP^{low}CD45^+TER119^-$ viable lymph node cells by confocal microscopy indicated that the GFPlow hematopoietic cells were indeed $CD45^+$ leukocytes (Fig. 3A and B). In contrast, the isolated $GFP^{high}CD45^-TER119^-$ viable lymph node cells were $CD45^-$ and therefore non-hematopoietic (Fig. 3A and B). In order to further characterize the GFP^{low} and GFP^{high} cells, we generated bone marrow chimera mice to distinguish donor bone-marrow-derived hematopoietic cells from host non-hematopoietic cells. For this purpose, T-cell-depleted bone marrow cells from αSMA-GFP-transgenic mice ($CD45.1^-CD45.2^+$) were transferred into lethally irradiated B6-Ly5.1 mice ($CD45.1^+CD45.2^-$). We designated these bone marrow chimera mice as GFP > Ly5.1 mice (Fig. 3C). Simultaneously, T-cell-depleted bone marrow cells from B6-Ly5.1 mice were transferred into lethally irradiated αSMA-GFP-transgenic mice, and these bone marrow chimera mice were designated as Ly5.1 > GFP mice (Fig. 3C). The analysis of GFP expression in enzyme-digested lymph node cells revealed that GFP^{low} cells were detectable in both GFP > Ly5.1 and Ly5.1 > GFP mice, whereas GFPhigh cells were detectable in only Ly5.1 > GFP mice (Fig. 3C top panels). The GFP^{low} cells in GFP > Ly5.1 mice were exclusively $CD45.1^-CD45.2^+$ and were therefore derived from bone marrow hematopoietic cells (Fig. 3C bottom panels), reconfirming that αSMA-GFP^{low} lymph node cells contained cells of hematopoietic origin. In contrast, the GFP^{low} cells in Ly5.1 > GFP mice were a mixture of $CD45.1^+CD45.2^-$ donor bone-marrow-derived leukocytes, $CD45.1^-CD45.2^+$ host irradiation-resistant leukocytes, and $CD45.1^-CD45.2^-$ host non-hematopoietic cells (Fig. 3C bottom panels). These results indicated that the αSMA-GFP^{low} lymph node cells were indeed a mixture of host non-hematopoietic cells and donor hematopoietic cells that acquired GFP proteins from host cells, whereas the αSMA-GFP^{high} lymph node cells were exclusively non-hematopoietic.

The αSMA-GFP^{low} hematopoietic cells detected in either combination of the bone marrow chimera mice were $CD11b^+CD11c^+I\text{-}A^{b+}$ (Fig. 3D), resembling macrophages. It was likely that these macrophages in the lymph nodes acquired GFP proteins from non-hematopoietic αSMA-GFP^+ cells.

3.4. Molecular expression profiles of αSMA-GFP^+ non-hematopoietic cell subpopulations

Finally, we examined the molecular expression profiles of αSMA-GFP^+ cells in $gp38^-CD31^-$ and $gp38^-CD31^+$ non-hematopoietic ($CD45^-TER119^-$) lymph node cells. As shown in Fig. 4A, flow cytometric analysis of cell-surface proteins revealed that αSMA-GFP^+ and αSMA-GFP^- subpopulations in $gp38^-CD31^-$ non-hematopoietic lymph node cells had quite dissimilar expression profiles of cell-surface molecules. In contrast, αSMA-GFP^+ and αSMA-GFP^- subpopulations in $gp38^+CD31^-$ non-hematopoietic lymph node cells had very similar expression profiles of cell-surface molecules (Fig. 4A). Indeed, the expression profiles of the cell-surface molecules were similar among αSMA-GFP^+ $gp38^-CD31^-$, αSMA-GFP^+ $gp38^+CD31^-$, and αSMA-GFP^- $gp38^+CD31^-$ subpopulations in non-hematopoietic lymph node cells, although the expression profiles of CD140a, $I\text{-}A^b$, and CD90 were distinct between αSMA-GFP^+ $gp38^-CD31^-$ subpopulation and αSMA-GFP^+ $gp38^+CD31^-$ and αSMA-GFP^- $gp38^+CD31^-$ subpopulations (Fig. 4A). The αSMA-GFP^- $gp38^-CD31^-$ non-hematopoietic cell subpopulation differed from the three other subpopulations in the expression of the cell-surface molecules examined (Fig. 4A). These molecular expression profiles suggested similarities between $\alpha SMA^+gp38^{+-}CD31^-$ and $\alpha SMA^-gp38^+CD31^-$ subpopulations of lymph node non-hematopoietic cells, and dissimilarities between $\alpha SMA^+gp38^-CD31^-$ and $\alpha SMA^-gp38^-CD31^-$ lymph node non-hematopoietic subpopulations.

We further isolated αSMA-GFP^- $gp38^-CD31^-$, αSMA-GFP^{+-} $gp38^-CD31^-$, αSMA-GFP^- $gp38^+CD31^-$, and αSMA-GFP^+gp38^{+-} $CD31^-$ non-hematopoietic lymph node cell subpopulations with a cell sorter and examined the expression of various mRNAs by quantitative RT-PCR analysis. The expression profiles of Acta2 (αSMA), GFP, and Pdpn (podoplanin, gp38) verified the successful isolation of the indicated cell subpopulations (Fig. 4B). Like Acta2, genes encoding conventional PVC markers, such as SM22, RGS5,

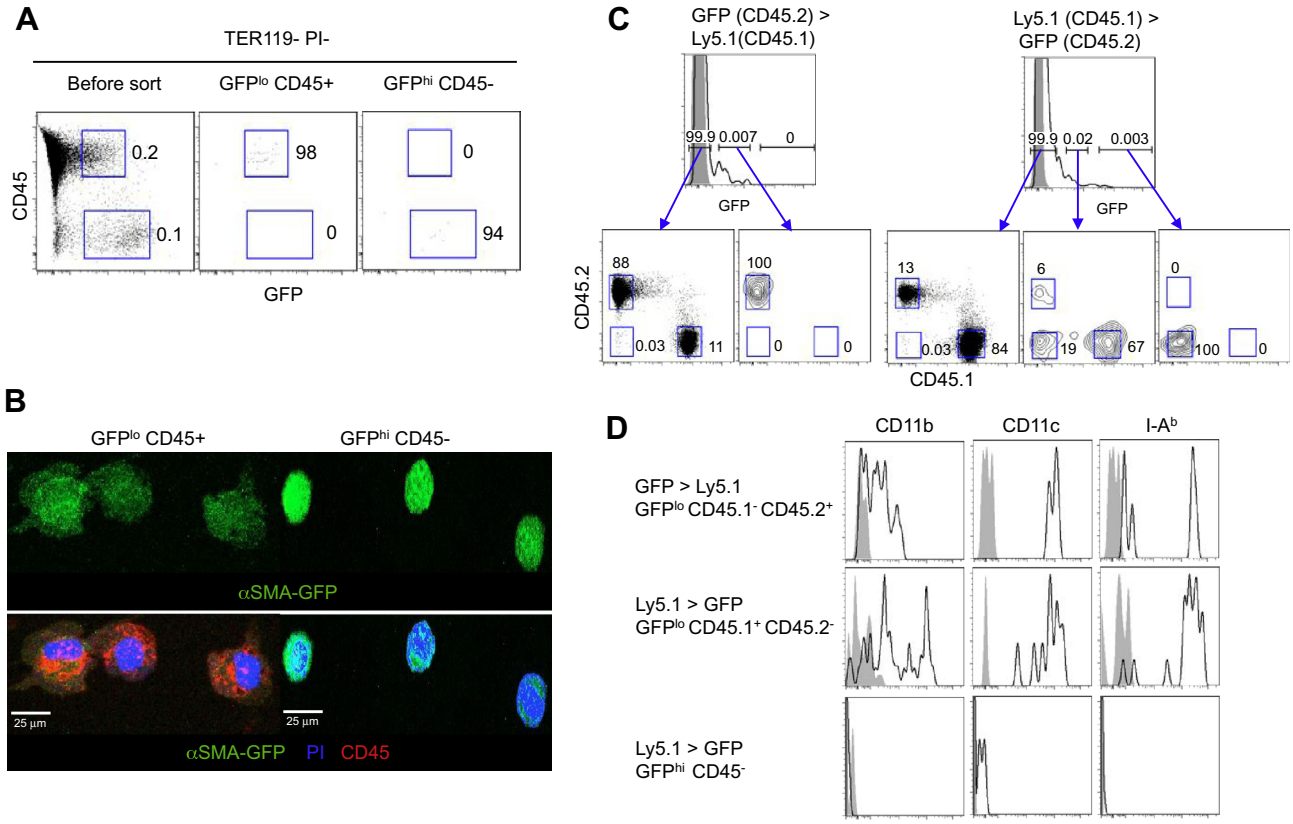

Fig. 3. Analysis of αSMA-GFP^{low} cells. (A) Representative flow cytometry profiles of CD45 and GFP in TER119$^-$PI$^-$ non-erythroid viable cells. Lymph node cells from 10-week-old αSMA-GFP-transgenic mice (left) were sorted for GFP^{low}CD45$^+$ cells (middle) and GFP^{high}CD45$^-$ cells (right). Numbers indicate frequency of cells within indicated boxes. (B) GFP^{low}CD45$^+$ cells and GFP^{high}CD45$^-$ cells isolated in (A) were multi-color analyzed for GFP (green), CD45 (red), and nuclei (PI, blue) by confocal microscopy. Shown are images for GFP alone (top) and GFP, CD45, and PI (bottom). (C) Flow cytometric analysis of TER119$^-$PI$^-$ non-erythroid viable lymph node cells from indicated bone marrow chimera mice. Shaded areas denote control profiles of the cells from B6 mice. (D) Flow cytometric analysis of indicated cells for cell-surface expression of CD11b, CD11c, and I-A^b. Shaded profiles represent control profiles stained with isotype control antibodies. Data are representative of three independent experiments.

and NG2, showed higher expression in αSMA-GFP$^+$ than αSMA-GFP$^-$ subpopulations of individual non-hematopoietic cells (Fig. 4B), in agreement with the successful purification of αSMA-GFP$^+$ and αSMA-GFP$^-$ subpopulations. The fact that the PVC-associated genes were most strongly expressed in αSMA-GFP$^+$gp38$^-$CD31$^-$ non-hematopoietic lymph node cells indicated that this population was enriched with PVCs. Whereas the expression of NG2 was detected in only gp38$^-$CD31$^-$ cells, the FRC-associated gene IL7 was specifically detected in gp38$^+$CD31$^-$ cells (Fig. 4B), suggesting that gp38$^-$CD31$^-$ and gp38$^+$CD31$^-$ cells are functionally distinct, irrespective of the expression of αSMA-GFP.

Chemokines are important for the regulation of trafficking and localization of immune cells in the lymph nodes. Interestingly, the expression of chemokine genes, including CCL2, CCL19, CCL25, CXCL14, and CX3CL1, was significantly different between αSMA-GFP$^+$ and αSMA-GFP$^-$ subpopulations of gp38$^+$CD31$^-$ non-hematopoietic cells, whereas the expression of CCL3, CCL19, CXCL1, CXCL2, and CXCL10 genes was significantly different between αSMA-GFP$^+$ and αSMA-GFP$^-$ subpopulations of gp38$^-$CD31$^-$ non-hematopoietic cells (Fig. 4C). Thus, the positive and negative expression of αSMA-GFP revealed functionally distinct subpopulations in gp38-CD31$^-$ and gp38$^+$CD31$^-$ non-hematopoietic lymph node cells.

4. Discussion

The present results indicate that αSMA expression can identify hitherto unknown subpopulations of non-hematopoietic cells in the lymph nodes of αSMA-GFP-transgenic mice. The gp38$^+$CD31$^-$ non-hematopoietic lymph node cells, previously known to contain FRCs, can be clearly subdivided into αSMA$^+$ and αSMA$^-$ subpopulations that are similar in regard to the expression of several cell-surface molecules but different in terms of chemokine gene expression. The gp38$^-$CD31$^-$ non-hematopoietic lymph node cells, which contain PVCs, can also be clearly subdivided into αSMA$^+$ and αSMA$^-$ subpopulations that differ in the expression of cell-surface molecules and chemokine genes. Given growing evidence suggesting that lymph node non-hematopoietic cells are highly heterogeneous [8], the clear-cut positive and negative expression of αSMA reported in this study is a useful tool for the further characterization of non-hematopoietic cells in the lymph nodes.

The present results also indicate that GFP^{low} cells in the lymph nodes of αSMA-GFP-transgenic mice include a fraction of hematopoietic cells. Bone marrow chimera experiments reconfirmed that these cells are hematopoietic and likely macrophages that have acquired GFP proteins from GFP^{high} αSMA$^+$ non-hematopoietic cells. Such activity by a fraction of hematopoietic cells, particularly macrophages, should be carefully considered in future analysis of non-hematopoietic cells in the lymph nodes.

It has been shown that αSMA$^+$ PVCs contain multipotent cells capable of differentiating into other cell types such as osteoblasts and adipocytes [4,9,10]. During tissue injury, PVCs in various organs are known to differentiate into αSMA$^+$ myofibroblasts to facilitate injury repair, tissue remodeling, and fibrosis by producing extracellular matrix components [10–14]. It is still unclear which αSMA$^+$ lymph node cell subpopulation possesses such progenitor potential. In this regard, it is important to delineate the characteristics of the multiple αSMA$^+$ lymph node cell subpopulations described in this study.

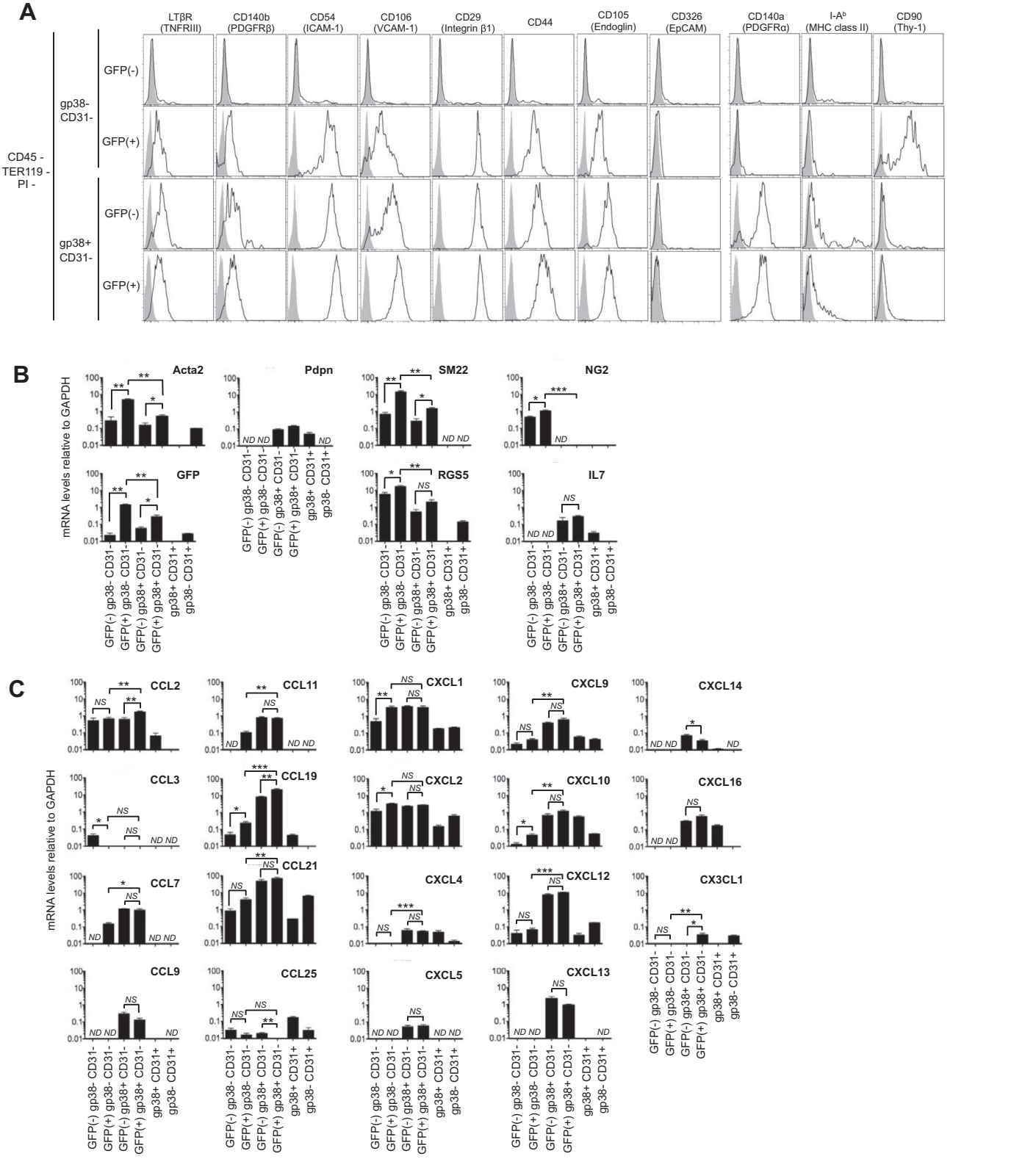

Fig. 4. (A) Flow cytometric analysis of αSMA$^+$ and αSMA$^-$ non-hematopoietic lymph node cell subpopulations. Indicated lymph node cell subpopulations from 8- to 10-week-old αSMA-GFP-transgenic mice were analyzed for the expression of indicated cell-surface molecules. Shaded areas denote control staining of the cells stained with normal rat IgG. Shown are representative results from three independent experiments. (B) Quantitative RT-PCR analysis of αSMA$^+$ and αSMA$^-$ non-hematopoietic lymph node cell subpopulations. Indicated lymph node cell subpopulations from 8- to 11-week-old αSMA-GFP-transgenic mice were analyzed for the expression of indicated genes by quantitative RT-PCR. GFP(+) and GFP(−) represent αSMA-GFP$^+$ and αSMA-GFP$^-$, respectively. mRNA levels were normalized to the housekeeping GAPDH mRNA level. Data represent means and SEs of three independent measurements. (C) Quantitative RT-PCR analysis of chemokine gene expression. Indicated lymph node cell subpopulations from 8- to 11-week-old αSMA-GFP-transgenic mice were analyzed for the expression of indicated genes by quantitative RT-PCR. GFP(+) and GFP(−) represent αSMA-GFP$^+$ and αSMA-GFP$^-$, respectively. mRNA levels were normalized to the housekeeping GAPDH mRNA level. Data represent means and SEs of three independent measurements. Among the genes examined (listed in Supplementary Table S1), CCL1, CCL4, CCL5, CCL6, CCL8, CCL12, CCL17, CCL20, CCL22, CCL24, CCL27, CCL28, Cinc2-like, CXCL7, CXCL11, CXCL15, and XCL1 were not detected in any of the cell subpopulations analyzed. Statistical comparison was performed with the Student's *t*-test. $^*p < 0.05$; $^{**}p < 0.01$; $^{***}p < 0.001$; NS, not significant ($p \geqslant 0.05$); ND, not detectable.

In conclusion, we have identified hitherto unknown subpopulations of lymph node non-hematopoietic cells, by the use of αSMA-GFP-transgenic mice. Our findings are expected to be useful for the further characterization of non-hematopoietic cells in immune organs, in an attempt to understand the development, maintenance, and regulation of the immune system.

Acknowledgments

The authors thank Drs. Sanai Sato (National Eye Institute) and Ivo Kalajzic (University of Connecticut Health Center) for providing αSMA-GFP-transgenic mice, and Drs. Mie Sakata and Izumi Ohigashi and other members of the laboratory for support in experiments and discussion. This study was supported by Grants-in-Aid for Scientific Research from MEXT and JSPS (23249025, 24111004, and 25111507), Japan.

Appendix A. Supplementary data

Supplementary data associated with this article can be found, in the online version, at http://dx.doi.org/10.1016/j.bbrc.2014.05.023.

References

[1] A. Link, T.K. Vogt, S. Favre, M.R. Britschgi, H. Acha-Orbea, B. Hinz, J.G. Cyster, S.A. Luther, Fibroblastic reticular cells in lymph nodes regulate the homeostasis of naive T cells, Nat. Immunol. 8 (2007) 1255–1265.
[2] T.H. Pham, P. Baluk, Y. Xu, I. Grigorova, A.J. Bankovich, R. Pappu, S.R. Coughlin, D.M. McDonald, S.R. Schwab, J.G. Cyster, Lymphatic endothelial cell sphingosine kinase activity is required for lymphocyte egress and lymphatic patterning, J. Exp. Med. 207 (2010) 17–27.
[3] V. Nehls, D. Drenckhahn, Heterogeneity of microvascular pericytes for smooth muscle type alpha-actin, J. Cell Biol. 113 (1991) 147–154.
[4] M. Crisan, M. Corselli, W.C. Chen, B. Péault, Perivascular cells for regenerative medicine, J. Cell. Mol. Med. 16 (2012) 2851–2860.
[5] M.F. Toccanier-Pelte, O. Skalli, Y. Kapanci, G. Gabbiani, Characterization of stromal cells with myoid features in lymph nodes and spleen in normal and pathologic conditions, Am. J. Pathol. 129 (1987) 109–118.
[6] T. Yokota, Y. Kawakami, Y. Nagai, J.X. Ma, J.Y. Tsai, P.W. Kincade, S. Sato, Bone marrow lacks a transplantable progenitor for smooth muscle type alpha-actin-expressing cells, Stem Cells 24 (2006) 13–22.
[7] A.L. Fletcher, D. Malhotra, S.E. Acton, V. Lukacs-Kornek, A. Bellemare-Pelletier, M. Curry, M. Armant, S.J. Turley, Reproducible isolation of lymph node stromal cells reveals site-dependent differences in fibroblastic reticular cells, Front. Immunol. 2 (2011) 35.
[8] M. Buettner, R. Pabst, U. Bode, Stromal cell heterogeneity in lymphoid organs, Trends Immunol. 31 (2010) 80–86.
[9] M.J. Doherty, B.A. Ashton, S. Walsh, J.N. Beresford, M.E. Grant, A.E. Canfield, Vascular pericytes express osteogenic potential in vitro and in vivo, J. Bone Miner. Res. 13 (1998) 828–838.
[10] Y. Tintut, Z. Alfonso, T. Saini, K. Radcliff, K. Watson, K. Boström, L.L. Demer, Multilineage potential of cells from the artery wall, Circulation 108 (2003) 2505–2510.
[11] L. Rønnov-Jessen, O.W. Petersen, A function for filamentous alpha-smooth muscle actin: retardation of motility in fibroblasts, J. Cell Biol. 134 (1996) 67–80.
[12] S. Dulauroy, S.E. Di Carlo, F. Langa, G. Eberl, L. Peduto, Lineage tracing and genetic ablation of ADAM12(+) perivascular cells identify a major source of profibrotic cells during acute tissue injury, Nat. Med. 18 (2012) 1262–1270.
[13] V.S. LeBleu, G. Taduri, J. O'Connell, Y. Teng, V.G. Cooke, C. Woda, H. Sugimoto, R. Kalluri, Origin and function of myofibroblasts in kidney fibrosis, Nat. Med. 19 (2013) 1047–1053.
[14] J. Davis, J.D. Molkentin, Myofibroblasts: trust your heart and let fate decide, J. Mol. Cell. Cardiol. (2013), <http://dx.doi.org/10.1016/j.yjmcc.2013.10.019>.